Check for updates

View Article Online
View Journal

Energy & Environmental Science

Accepted Manuscript

This article can be cited before page numbers have been issued, to do this please use: C. Pan, L. N. Y. Cao, J. Meng, L. Jia, W. Hu, Z. L. Wang and X. Pu, *Energy Environ. Sci.*, 2024, DOI: 10.1039/D3EE03496H.

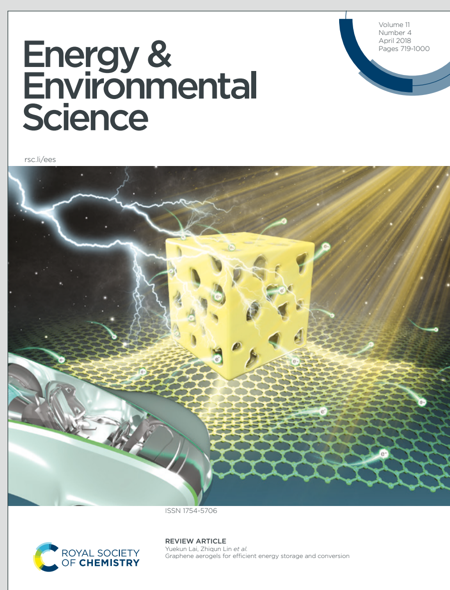

This is an Accepted Manuscript, which has been through the Royal Society of Chemistry peer review process and has been accepted for publication.

Accepted Manuscripts are published online shortly after acceptance, before technical editing, formatting and proof reading. Using this free service, authors can make their results available to the community, in citable form, before we publish the edited article. We will replace this Accepted Manuscript with the edited and formatted Advance Article as soon as it is available.

You can find more information about Accepted Manuscripts in the Information for Authors.

Please note that technical editing may introduce minor changes to the text and/or graphics, which may alter content. The journal's standard Terms & Conditions and the Ethical guidelines still apply. In no event shall the Royal Society of Chemistry be held responsible for any errors or omissions in this Accepted Manuscript or any consequences arising from the use of any information it contains.

ROYAL SOCIETY OF CHEMISTRY

rsc.li/ees

View Article Online
DOI: 10.1039/D3EE03496H

Field Effect Nanogenerator as Operated by Sliding Gates

Chongxiang Pan‡, Leo N.Y. Cao‡, Jia Meng‡, Luyao Jia, Weiguo Hu, Zhong Lin Wang and Xiong Pu

Published on 21 December 2023. Downloaded by the Georgia Tech Library on 1/2/2024 8:42:12 PM.

Energy & Environmental Science Accepted Manuscript

Broader context

Extracting electricity from semiconductor materials through the excitation of charge carriers or manipulation of carrier population/transport has been realized in many energy devices, such as thermoelectric generators, photovoltaic devices, and so on. However, utilizing materials' semiconducting effect for mechanoelectrical energy conversion is still limited due to the lack of strategies to modulate the carrier's transport by mechanical motion. Here, we report a mechanoelectric energy conversion mechanism by coupling the triboelectrification effect and electrostatic field effect, achieving electricity generation in the semiconductor channel as operated by the mechanical energy input through a sliding gate. This electricity generator can output electricity waveform following well with the sliding speed of the gate, yielding high voltage, high charge density and 3-fold higher power density than a conventional electrostatic induction-based triboelectric nanogenerator. Furthermore, the strategy to achieve dynamical and regional doping of semiconductors via a sliding-gate induced electrostatic field could be also promising for developing new devices for micro-electro-mechanical system.

View Article Online
DOI: 10.1039/D3EE03496H

Field Effect Nanogenerator as Operated by Sliding Gates

Chongxiang Pan,[a, b, ‡] *Leo N.Y. Cao,* [b, c, ‡] *Jia Meng,* [a, b, ‡] *Luyao Jia,*[b, c] *Weiguo Hu,* [a, b, c] *Zhong Lin Wang,*[b, c, d,] *and Xiong Pu*[a, b, c,]

[a] Center on Nanoenergy Research, School of Physical Science and Technology, Guangxi University, Nanning 530004, P. R. China.

[b] CAS Center for Excellence in Nanoscience, Beijing Key Laboratory of Micro-nano Energy and Sensor, Beijing Institute of Nanoenergy and Nanosystems, Chinese Academy of Sciences, Beijing 101400, P. R. China.

[c] School of Nanoscience and Engineering, University of Chinese Academy of Sciences, Beijing 100049, P. R. China.

[d] School of Materials Science and Engineering, Georgia Institute of Technology, Atlanta, Georgia 30332-0245, USA.

† Electronic supplementary information (ESI) available.

‡ These authors contributed equally: Chongxiang Pan, Leo N.Y. Cao, Jia Meng.

 Corresponding authors: Zhong Lin Wang, Xiong Pu

E-mail: puxiong@binn.cas.cn, zlwang@gatech.edu

Published on 21 December 2023. Downloaded by the Georgia Tech Library on 1/2/2024 8:42:12 PM.

Energy & Environmental Science Accepted Manuscript

View Article Online
DOI: 10.1039/D3EE03496H

Published on 21 December 2023. Downloaded by the Georgia Tech Library on 1/2/2024 8:42:12 PM.

Energy & Environmental Science Accepted Manuscript

Abstract

Controlling the motion of charge carriers in semiconductor materials is the fundamental strategy to realize many functional devices, which is typically done by applying an external voltage source. Here, using the electrostatic potential generated by a triboelectric material that is taken as a sliding "gate", functional current is generated across a semiconductor channel when the gate is moving in parallel to the dielectric surface. Systematic studies verify that the motion of the electrified "gate" induces the regional and dynamical doping of the semiconductor channel, and thereby drives the carrier transport without applying an external voltage. This sliding-gated generator realizes mechanoelectric energy conversion based on coupled triboelectrification effect and electrostatic field effect, and is therefore termed as a field effect nanogenerator (FENG). It can output electrical currents with waveform following well with the gate's sliding speed, which makes it different from conventional induction-based triboelectric nanogenerators with instantaneous outputs. Meantime, it can yield 3 times higher averaged power density than that of a sliding-mode triboelectric nanogenerator. Moreover, a rotary FENG is designed for practically viable direct-current generation. This work presents an undiscovered strategy for carrier manipulation in semiconductors, demonstrating a promising mechanoelectric energy conversion mechanism and a practical self-powered device.

View Article Online
DOI: 10.1039/D3EE03496H

Broader context

Extracting electricity from semiconductor materials through the excitation of charge carriers or manipulation of carrier population/transport has been realized in many energy devices, such as thermoelectric generators, photovoltaic devices, and so on. However, utilizing materials' semiconducting effect for mechanoelectrical energy conversion is still limited due to the lack of strategies to modulate the carrier's transport by mechanical motion. Here, we report a mechanoelectric energy conversion mechanism by coupling the triboelectrification effect and electrostatic field effect, achieving electricity generation in the semiconductor channel as operated by the mechanical energy input through a sliding gate. This electricity generator can output electricity waveform following well with the sliding speed of the gate, yielding high voltage, high charge density and 3-fold higher power density than a conventional electrostatic induction-based triboelectric nanogenerator. Furthermore, the strategy to achieve dynamical and regional doping of semiconductors via a sliding-gate induced electrostatic field could be also promising for developing new devices for micro-electro-mechanical system.

Published on 21 December 2023. Downloaded by the Georgia Tech Library on 1/2/2024 8:42:12 PM.

Energy & Environmental Science Accepted Manuscript

View Article Online
DOI: 10.1039/D3EE03496H

Published on 21 December 2023. Downloaded by the Georgia Tech Library on 1/2/2024 8:42:12 PM.

Energy & Environmental Science Accepted Manuscript

Introduction

Controllable manipulation of charge carriers is important for exploring fundamental electronic properties of materials and practical applications of desired functional devices[1-3]. The electrostatic doping, as a promising alternative to the chemical doping in which foreign atom impurities are involved, allows controllable and reversible changes of carrier population without producing disorders in materials, providing an opportunity for controlling material properties, such as superconductivity[4, 5], insulating-metal transition[6, 7], magnetic phase transition[8, 9] and exciton dynamics[10, 11]. The electric field for electrostatic doping is usually provided by an external voltage applied on the gate electrode[4, 5, 9-11], or by the electric double layer (EDL) formed at the interface between electrolyte and gate electrode[7, 8], or by the polarized interface at the oxide heterostructures[6]. Nevertheless, these methods either require large voltage to polarize the dielectrics, or may introduce impurities due to the undesired interfacial electrochemical reactions. Meantime, to drive the transport of charge carriers, another source-drain voltage is required, which is the fundamental of field-effect transistors. Therefore, seeking undiscovered strategies to realize the electrostatic modulation and transport of charge carriers could lead to exploring new functional devices.

Triboelectrification is an ancient universal phenomenon generating electrostatic field, which recently attracts a wide-range interest to explore its underlying mechanism and potential applications[12-14]. Thousands of volt-high surface potential can be easily obtained from the injection of tribo-charges with opposite polarities into two different materials after the contact-electrification process[15, 16]. This huge electrostatic potential has been demonstrated to generate microplasma[17], actuate electroresponsive polymers[18], manipulate droplet transport[19, 20],

View Article Online
DOI: 10.1039/D3EE03496H

provide ionization charges for mass spectrometer[21], implement air cleaning due to electrostatic adsorption[22], and so on. Conceivably, this tremendous surface potential can replace the gate voltage to electrostatically modulate the population of charge carriers in semiconductor materials[23, 24], but the modulation process is still limited due to the need of external source-drain voltage to drive the transport of charge carriers.

Here, we proposed a novel strategy to modulate the carrier population and drive the transport of charge carriers simultaneously via a sliding-gate induced electrostatic field, not only realizing the dynamical and regional doping of semiconductors, but also resulting in the electricity generation in the semiconductor channel along the sliding motion direction, as depicted in Fig. 1a. The sliding gate produces electrified static charges at the interfaces, the electrostatic field of which is dynamically changing and unevenly distributed. Then, the triboelectric gate induces the regional and dynamical doping of the semiconductor "channel" and also generates electricity through an external circuit. For better understanding, we can compare our device to a field-effect transistor (FET, Fig. 1b). The differences include that: (1) there is no external gate electrode to apply gate voltage, but a slider exerting uneven electrostatic potential; (2) The source-drain voltage is also not needed. The transport of carriers is driven by the sliding gate, and the electricity can be directly generated between "source" and "drain" electrodes, rather than sourcing voltage for measuring current (Fig. 1c). This field-effect nanogenerator (FENG), based on coupled triboelectric effect and electrostatic field effect, can not only transform the FET device to mechanical energy harvesting device, but also output about 3 times higher average power density than a conventional sliding-mode triboelectric nanogenerator (S-TENG) without the underlying semiconductor channel. Furthermore, we

Published on 21 December 2023. Downloaded by the Georgia Tech Library on 1/2/2024 8:42:12 PM.

Energy & Environmental Science Accepted Manuscript

View Article Online
DOI: 10.1039/D3EE03496H

design a practically viable rotary FENG for direct-current (DC) outputs. Therefore, our work presents a novel strategy for carriers' manipulation in semiconductors, provides a new mechanoelectric energy conversion mechanism, and reports practical devices potentially as power sources or self-powered sensors.

Published on 21 December 2023. Downloaded by the Georgia Tech Library on 1/2/2024 8:42:12 PM.

Energy & Environmental Science Accepted Manuscript

Results and discussion

The structure and electric outputs of the FENG

The device structure of the FENG is schematically shown in Fig. 1a, where a PTFE film is attached on the surface of Si and a nylon slider is sliding on the top. The Si used here is close to the intrinsic Si without intentionally doped impurities, the resistivity of which is larger than 100 kOhm cm. The Copper (Cu) was deposited onto the left and right terminals of the Si through magnetron sputtering for the connection with the external circuit. The optical picture of a FENG is shown in Fig. S1 (ESI†). The Ohmic contact of Si with Cu electrodes was confirmed by the straight-line *I-V* curve obtained between the two electrodes (Fig. S2, ESI†). The characteristic of the electric output varies well with the motion forms of the slider. We define the right-side Cu electrode as the positive and the left as the negative. When the nylon slider moved unidirectionally from left to the right at a constant speed, direct current (DC) constant outputs were produced (red lines in Fig. 1d). It was observed that positive voltage and current were generated in external circuit when sliding the nylon from left to the right, and negative electrical outputs were obtained when sliding from right to the left (blue and green lines in Fig. 1d). Alternative current (AC) outputs were then generated if the nylon slider slid on the PTFE film back and forth. The current and voltage both have very similar waveform with the sliding speed. Continuous electrical outputs can be obtained as long as the sliding

View Article Online
DOI: 10.1039/D3EE03496H

motion is not stopped, which makes it different from conventional TENGs where only pulse outputs can be acquired. In the following study, we choose the reciprocating sliding as the motion forms of the slider. During the reciprocating sliding of nylon slider (maximum sliding speed was 30 cm/s, sliding distance was 5 cm, and normal pressure was 22.2 kPa), the open-circuit voltage, short-circuit current and transferred charge quantity of the FENG could reach peak value of around 79 V, 10 μA and 576 nC, respectively (green lines in Fig. 1d).

A series of control devices were tested to demonstrate the characteristics of the FENG. When there is no Si layer (PTFE film attached on the acrylic plate directly with the electrodes on the two side surfaces), the electric outputs were much smaller than the FENG during the sliding of nylon on the PTFE film (Fig. S3, ESI†). When the Si was replaced by Cu, there was no voltage and current output during the slip of nylon film on the PTFE film (Fig. S4, ESI†), indicating that the high resistivity and semi-conductivity of Si were prerequisite for the electricity generation. The electrical outputs were also negligible when sliding PTFE or nylon slider directly on the Si (Fig. S5, ESI†). Furthermore, the electric outputs were also orders of magnitude smaller if two sliding materials were the same (either PTFE or nylon sliding by their own), as shown in Fig. S6 (ESI†).

A traditional sliding-mode triboelectric nanogenerator (S-TENG, as schemed by the inset of Fig. 1e) was also constructed as a control device for comparison. The short-circuit current and charge quantity of the FENG was approximately 12 and 6.4 times larger than that of the S-TENG, respectively (Fig. 1e), though the open-circuit voltage of the S-TENG could be higher (~114 V) (Fig. S7, ESI†). Meantime, the internal impedance (estimated by the matched external resistance) reduced from 80 MOhm of the S-TENG to about 500 KOhm of the FENG (Fig. 1f

Published on 21 December 2023. Downloaded by the Georgia Tech Library on 1/2/2024 8:42:12 PM.

Energy & Environmental Science Accepted Manuscript

View Article Online
DOI: 10.1039/D3EE03496H

and Fig. S8, ESI†). More importantly, the averaged power density of our device was about 3 times higher than that of the S-TENG (Fig. 1f), although their peak power densities were close (Fig. S9, ESI†). We then compared the transferred charge quantity per motion cycle of our device with representative sliding or rotating TENGs in literatures, as it was well accepted as an important parameter for performance evaluation. The charge density of the FENG device reaches 384 $\mu C/m^2$ calculated by the covered area of the sliding process of the slider, which is larger than most previous sliding or rotating TENGs using strategies like air breakdown[25-28], charge excitation[29-31], commercial film[32-35], or charge space accumulation[36, 37] (Fig. 1g and Table S1, ESI†). Furthermore, our FENG device can generate average power density comparable or even larger than previous sliding TENGs, but has the advantage of more lower internal impedance[30, 38-42] (Fig. 1h and Table S2, ESI†).

Evidences of dynamical and regional doping by electrostatic charges

A series of investigations were conducted to get insights into the mechanism of the FENG. Firstly, we simulated our device at the microscopic level by the COMSOL Multiphysics Software (Note S1, ESI†). The electrostatic potential originated from the triboelectrification between PTFE and nylon films was dynamically and regionally distributed with the sliding of nylon slider (Fig. S10 and Movie S1, ESI†). The uneven electrostatic potential caused by net electrostatic charges with opposite polarities in different regions was exerted on the underneath Si and induced regionally different electrostatic doping effects. Therefore, the hole concentration is low in the surface of Si right underneath the nylon slider (N-type doped region), but high in Si without nylon slider on top (P-type doped region), as confirmed by the simulation results (Fig. 2a and Movie S2, ESI†); whereas, the electron concentration distribution is in the

Published on 21 December 2023. Downloaded by the Georgia Tech Library on 1/2/2024 8:42:12 PM.

Energy & Environmental Science Accepted Manuscript

View Article Online
DOI: 10.1039/D3EE03496H

Published on 21 December 2023. Downloaded by the Georgia Tech Library on 1/2/2024 8:42:12 PM.

Energy & Environmental Science Accepted Manuscript

opposite (Fig. S11, ESI†). Hence, the distribution of different doped regions should vary accordingly with the slider (Fig. 2a). Furthermore, the time-varying profiles of hole concentration at the left terminal (x=0 μm) and right terminal (x=90 μm) were exhibited in Fig. 2b. The hole concentration increased from 1.69×10^{5} cm^{-3} to 4.38×10^{12} cm^{-3} at the left terminal when sliding the slider from left to right; whereas, the right terminal changed oppositely (hole concentration decreased from 4.41×10^{12} cm^{-3} to $9.85\times10^{5}cm^{-3}$) (Fig. 2b). Interestingly, this resulted in the variation of the hole concentration difference between the right and left terminals (changing from 4.41×10^{12} cm^{-3} to -4.38×10^{12} cm^{-3}) (Fig. 2c), which was the origination of the electricity generation when two electrodes connected through the external circuit.

Then, the uneven distribution of electrostatic potentials on PTFE and nylon films was confirmed experimentally by the surface potential measurements. The surface potential of pristine PTFE and nylon film before the triboelectrification was as low as -124 V and +30 V, respectively (Fig. S12, ESI†). After sliding the nylon slider on the PTFE film, the surface potential of PTFE and nylon film increased to -1.898 kV and +3.179 kV, respectively (Fig. S13, ESI†). The higher absolute value of the surface potential of nylon film is because of the smaller slider area than the PTFE area (slider is 3×3 cm^2, sliding distance is 5 cm, and the total PTFE sliding area is 3×8 cm^2). Since the total positive tribo-charges in nylon should be about the same as the negative tribo-charges in the PTFE, the tribo-charge density in slider (and therefore the absolute surface potential) should be higher than that of the PTFE film. As a result, the total surface potential should be uneven in different regions: the PTFE area without nylon slider on top (non-contact region, region i and iii) has net negative tribo-charges and surface potential of roughly -1.898 kV; whereas, the PTFE area with nylon slider on top

View Article Online
DOI: 10.1039/D3EE03496H

(contact region, region ii) has net positive tribo-charges and surface potential of roughly +1.280 kV (Fig. 2d). This regional distribution of electrostatic potential was well accordant with the COMSOL simulation.

To experimentally confirm the regional doping effect, we probed the carrier type on the surface of Si in different regions through measuring the diffusion of hot carriers (Fig. S14 and Note S2, ESI†). For all measurements, the positive terminal of an electrometer was connected to the hot probe. The Si underneath the non-contact region showed negative potential, correspondent to the holes as majority carriers; whereas, the Si underneath the contact region had positive potential and therefore the electrons as majority carriers (Fig. 2e).

The regional doping could also be reflected by the conductance (or *I-V* curve) between the two Cu electrodes of the Si. If the Si was uniformly exerted with electrostatic potential (two dielectric films were electrified and then the slider was taken away), an obvious increase in conductance was observed (state 2 in Fig. 2f), since the single type of majority carrier concentration should be increased throughout the surface channel. However, the conductance reduced to be even smaller than the original level, if the electrified slider was put back in the middle (state 3 in Fig. 2f). For the latter case, energy barrier could be formed across the surface regions with different types of electrostatic doping (see below discussion as well).

Furthermore, multi-alternate doping effect can be induced by increasing the slider numbers aligned in parallel. For demonstration, P-N-P-N-P doped regions in alternate arrays were constructed by two nylon sliders (Fig. 2g), which was verified by the hot-point probe measurement as shown in Fig. 2h.

When nylon film was attached on the Si and PTFE was as the slider, the dynamical and

Published on 21 December 2023. Downloaded by the Georgia Tech Library on 1/2/2024 8:42:12 PM.

Energy & Environmental Science Accepted Manuscript

View Article Online
DOI: 10.1039/D3EE03496H

regional doping was in opposite due to the opposite electrostatic potential (Fig. S15 and S16, ESI†).

The mechanism for the electrostatic doping and electricity generation

Based on above evidences, we propose that the electricity generation of our FENG device is originated from the regional and dynamical modulation of carrier transport in Si by the sliding-motion-induced variation of the uneven electrostatic potentials. We speculate the underlying mechanism for the electrostatic doping and electricity generation as follows (Fig. 3). At the static state, the nylon slider and PTFE film are firstly tribo-electrified with about the same amount of opposite electrostatic charges but different charge densities, so the electrostatic potential exerted on the Si will be uneven according to Gauss' Law (Fig. 3a and Note S3, ESI†). For the Si underneath non-contact region, electrons are repelled away and holes accumulated to the surface, leading to the band bending upwards and therefore the P-type doping (Fig. 3b); for the contact region, excessive electrons accumulate to the surface, resulting in the band bending downwards and the N-type doping (Fig. 3c). That means the Si "channel" consists of an N-doped region sandwiched by P-doped regions (Fig. 3d), which differs from a conventional FET with single-type doped channel. It should be noted that the energy barrier at the interfaces of the P-N region is forced by the electrostatic filed of electrified PTFE/nylon films, rather than the internal build-in electric field of traditional PN junction (Fig. S17 and Note S4, ESI†).

At the dynamic state, the position of the N-doped region should change accordingly with the position of the top nylon slider (Fig. 3e). When the nylon slider slides forwards, the electron carriers at the rear side of the slider will be drifted forwards by the Coulomb interaction with the positive static charges on the nylon slider and the static negative charges on the newly

Published on 21 December 2023. Downloaded by the Georgia Tech Library on 1/2/2024 8:42:12 PM.

Energy & Environmental Science Accepted Manuscript

View Article Online
DOI: 10.1039/D3EE03496H

exposed PTFE film. Meanwhile, the forward diffusion of hole carriers in the P-doped region behind the slider occurs due to the concentration difference between the preexisting P-doped region and newly exposed region. In the front of slider, the hole carriers will be also drifted to the ahead P-doped region by the net positive charges of the nylon slider and then diffuses forward (Fig. 3e, f). Therefore, electrons flow from the left to the right electrodes through the external load to balance the charges. The current generation will continue as long as the slider keeps sliding, and the current direction will be reversed if the sliding direction is reversed, which are two characteristics accordant with the experimental observations. Meantime, the dynamical and regional doping is the opposite process when tribo-negative PTFE film is used as slider and tribo-positive nylon film is attached on the Si (Fig. S18 and Note S5, ESI†).

The influencing parameters of the FENG device

A simplified capacitor model is detailed in Fig. S19 and Note S6 (ESI†) for quantifying the electrical outputs of the FENG. Given the surface potential in PTFE film (V_{surf}), the short-circuit current and open-circuit voltage can be expressed:

$$I_{sc} = wv\frac{L}{l}\frac{\varepsilon}{d}V_{surf} \tag{1}$$

$$V_{oc} = wv\frac{L}{l}R_{Si}\frac{\varepsilon}{d}V_{surf} \tag{2}$$

where w and l are the width and length (the sliding is along the length direction and the width is perpendicular to the sliding direction) of the nylon slider; v is the sliding speed of the slider; L is the length of the PTFE film; R_{Si} is the resistance of the Si; ε, d and V_{surf} are the permittivity, thickness, and surface potential of the PTFE film, respectively. Therefore, the influences of sliding speed, normal pressure on the slider, sliding distance and Si resistivity on

Published on 21 December 2023. Downloaded by the Georgia Tech Library on 1/2/2024 8:42:12 PM.

Energy & Environmental Science Accepted Manuscript

View Article Online
DOI: 10.1039/D3EE03496H

the electrical outputs were systematically investigated for getting further insights into the device. For these tests, the sliding motion was reciprocating and the sliding speed was in triangle waveform. The open-circuit voltage and short-circuit current of the FENG increased with the peak sliding speed of nylon slider; while the transferred charge quantity per motion cycle showed only very slight variation with the sliding speed (Fig. 4a). These results are consistent with the capacitor model. Therefore, this device, other than as a power source, could also be promising for vibration or speed sensor in MEMS systems. The normal pressure on the slider also contributes to the output of FENG. At the peak sliding speed of 30 cm/s and sliding distance of 5 cm, the electric output of FENG increased with the increase of the normal pressure on the slider (Fig. S20, ESI†). This is because that severe triboelectrification between the nylon slider and PTFE film at the larger pressure results in higher electrostatic charge densities in the two dielectric films (Fig. S21, ESI†). The sliding distance of the slider also influences the electrical output of FENG due to the change of total tribo-charges. At the peak sliding speed of 30 cm/s and normal pressure of 22.2 kPa, the electric output of FENG boosted with the extension of sliding distance (Fig. 4b). Importantly, when the sliding distance increased to 140 mm, the transferred charge of FENG reached 1.44 μC, correspondent to the charge density of 1.6 mC/m^2 when calculated by dividing the area of the slider. Furthermore, the electric outputs of FENG could be improved by increasing the ratio of the entire length of the device and the length of the slider (increasing the total sliding distance or decreasing the length of the slider) (Fig. 4c).

The high resistivity of Si is crucial for the electricity generation of FENG. The voltage and current output of FENG with the resistivity of Si less than 10 kOhm cm and 5 kOhm cm

Published on 21 December 2023. Downloaded by the Georgia Tech Library on 1/2/2024 8:42:12 PM.

Energy & Environmental Science Accepted Manuscript

View Article Online
DOI: 10.1039/D3EE03496H

were only 0.03 V, 0.08 μA and 0.01 V, 0.05 μA respectively, which were orders of magnitudes less than that of 100 kOhm cm (Fig. 4d). This can be easily understood that the regional electrostatic doping effect could disappear as the chemical doping content in Si increases. The thickness of the PTFE film attached on the Si also affected the output due to its impediment of electric field penetrating the surface of Si (Fig. S22, ESI†). The durability of FENG was measured over long cycles. After 3000 cycles of sliding of slider on the PTFE film, the voltage of FENG had only slight degeneration and the PTFE film had no severe abrasion (Fig. 4e and Fig. S23, ESI†).

For the demonstration of FENG device, 30 LEDs and a 5 W bulb can be easily lighted up by the reciprocating sliding of nylon slider on the PTFE film (Fig. S24a and b, ESI†). With the help of a rectifier, the electricity generated can be stored in the capacitor and an electronic watch can be powered continuously (Fig. S24c and d, ESI†).

DC electricity generation

Direct current should be generated if the slider keeps sliding in one direction rather than back-and-forth, which is, however, hard to be implemented in practical. Therefore, we designed a disc type FENG device with the slider rotating on the PTFE film to explore the DC outputs. The disc type FENG device contains a stator consisting of two isolated semicircular Si covered by a PTFE film, and a rotator with a square nylon slider (Fig. 5a). Firstly, we decomposed the clockwise rotation process into four sub-processes, as depicted in the inset in Fig. 5b. When connecting the right sides of two semicircular Si directly and measuring the outputs at the left sides, three positive and one negative current peaks were observed, correspondent to the four sliding routes i-iv respectively (Fig. 5b and SI Fig. S25a, ESI†). For sub-process i and iii, DC

Published on 21 December 2023. Downloaded by the Georgia Tech Library on 1/2/2024 8:42:12 PM.

Energy & Environmental Science Accepted Manuscript

View Article Online
DOI: 10.1039/D3EE03496H

Published on 21 December 2023. Downloaded by the Georgia Tech Library on 1/2/2024 8:42:12 PM.

Energy & Environmental Science Accepted Manuscript

electricity was generated following the above discussed mechanism; however, two extra peaks (ii and iv) in opposite signs were also produced when the slider slides across the two semicircular Si, which follows the electrostatic induction mechanism of a traditional sliding-mode TENG. Therefore, a diode was connected to the right-side terminals of the two semicircular Si. Then, DC output can be obtained during the whole rotation process with the sacrifice of negative peak number iv (Fig. 5c and Fig. S25b, ESI†). With this circuit connection, DC outputs can be realized at rotary mechanical motions (Fig. 5d). When driving the disc type FENG device with a rotary motor at the rotating speed of 200 r min^{-1}, the DC output with peak values of 260 V and 22 μA can be obtained directly, and 174 LEDs can be easily lighted up (Fig. 5e). Different capacitors can be also charged readily (Fig. S26, ESI†), and a calculator can be powered continuously (Fig. 5f).

Conclusions

In summary, we reported a field effect nanogenerator for mechanoelectric energy conversion by modulating the carrier population and transport in semiconductor Si via a sliding gate. The Si channel of the FENG was regionally doped by triboelectrification-generated electrostatic charges at the gate, and the sliding motion of the gate further yielded the electricity generation due to the dynamical modulation of carriers' transport in the channel. Theoretical and experimental investigations were conducted to verify the electricity generation mechanism based on the coupled triboelectrification effect and electrostatic field effect. The influencing parameters on the electric outputs were then explored for the insights into the device characteristics. Finally, DC output was realized through appropriately designing a rotary generator. Our results demonstrated an outstanding strategy to electrostatically modulate the

View Article Online
DOI: 10.1039/D3EE03496H

electrical transport in semiconductors with tribo-charges, and presented mechanical energy harvesting devices potentially as power sources or self-powered sensors.

Experimental

Device fabrication

The FENG device was fabricated by attaching an 80 mm×40 mm×0.08 mm PTFE film on the Si with a dimension of 100 mm×40 mm×0.5 mm, exposing the left and right surface of Si. The 100 mm×60 mm acrylic plate was used for the support of Si. The resistivity of the Si used here was larger than 100 kOhm cm. The Si was cleaned by ultrasonic treatment with acetone, ethanol, and deionized water before used. After the adhesion of PTFE film on the Si, the copper was deposited on the left and right surface of Si by the magnetron sputtering with a mask covering the PTFE film. The copper wire was sticked on the deposited area with adhesive tape as electrodes for the connection to the external load. The slider was fabricated by gluing the nylon film with a dimension of 30 mm×30 mm on the acrylic plate with double side tape. The traditional sliding-mode TENG was fabricated as follows: The PTFE film was attached on the Si, exposing one side surface of Si for the deposition of copper by the magnetron sputtering with a mask. A copper film was attached on the back surface of nylon film as slider, sliding in and out of the PTFE film. Here, the Si only served as electrode, and output signals were generated between Cu electrode and Si electrode. The disc type FENG device was fabricated as follows: Two semicircular Si was obtained by dividing the 4-inch Si in half and supported by an acrylic plate with a gap between them. The PTFE film was adhered on the two isolated semicircular Si as the stator, and a square nylon slider was attached on the circular acrylic plate as the rotator.

Published on 21 December 2023. Downloaded by the Georgia Tech Library on 1/2/2024 8:42:12 PM.

Energy & Environmental Science Accepted Manuscript

View Article Online
DOI: 10.1039/D3EE03496H

Electrical measurement and characterization

The sliding and rotary operation was implemented by a linear motor (TSMV1201S) and a rotary motor. The open-circuit voltage, short-circuit current and transferred charge of the FENG were recorded by a programmable electrometer (Keithley Instruments model 6517b). The surface potential of PTFE and nylon film was measured by the Isoprobe electrostatic voltmeter (model 279). The I-V curve of the FENG was measured by the 2450 SourceMeter. The optical photograph of PTFE film was pictured by the metalloscope (Leica DM 2700 M).

Hot-point probe measurement for the determination of carriers' type

Three pair electrodes were deposited on the left, middle, and right regions of Si by the magnetron sputtering with a designed mask. Cu wires with a diameter of 100-μm were used for the connection with external circuit and for the conduction of heat. Then, PTFE (or nylon) film was attached on the Si, and nylon (or PTFE) slider was fabricated as mentioned above. The hot point was created by heating one of electrode pairs with a heated electric soldering iron. The output signals were recorded by the Fluke 117C True RMS Multimeter with the connection of hot electrode to the red line of multimeter (SI Appendix, Note S2 and Fig. S14).

Author contributions

C.P., X.P., and Z.L.W. conceived the idea. C.P., and J.M. performed the experiments. C.P., and L.N.Y.C. performed the simulation process. L.J., and W.H. contributed to data analysis. C.P., X.P. and Z.L.W. wrote the paper with input from all authors.

Conflicts of interest

There are no conflicts to declare.

Published on 21 December 2023. Downloaded by the Georgia Tech Library on 1/2/2024 8:42:12 PM.

Energy & Environmental Science Accepted Manuscript

View Article Online
DOI: 10.1039/D3EE03496H

Acknowledgements

This work thanks for the support from the National Key R&D Project from Minister of Science and Technology (2021YFA1201603) and the National Natural Science Foundation of China (52173274).

References

1. C. H. Ahn, A. Bhattacharya, M. Di Ventra, J. N. Eckstein, C. D. Frisbie, M. E. Gershenson, A. M. Goldman, I. H. Inoue, J. Mannhart, A. J. Millis, A. F. Morpurgo, D. Natelson and J.-M. Triscone, *Rev. Mod. Phys.*, 2006, **78**, 1185-1212.
2. Y. Wu, D. Li, C.-L. Wu, H. Y. Hwang and Y. Cui, *Nat. Rev. Mater.*, 2022, **8**, 41-53.
3. P. Liu, B. Lei, X. Chen, L. Wang and X. Wang, *Nat. Rev. Phys.*, 2022, **4**, 336-352.
4. E. Sajadi, T. Palomaki, Z. Fei, W. Zhao, P. Bement, C. Olsen, S. Luescher, X. Xu, J. A. Folk and D. H. Cobden, *Science*, 2018, **362**, 922-925.
5. V. Fatemi, S. Wu, Y. Cao, L. Bretheau, Q. D. Gibson, K. Watanabe, T. Taniguchi, R. J. Cava and P. Jarillo-Herrero, *Science*, 2018, **362**, 926-929.
6. S. Raghavan, J. Y. Zhang, O. F. Shoron and S. Stemmer, *Phys. Rev. Lett.*, 2016, **117**, 037602.
7. J. Jeong, N. Aetukuri, T. Graf, T. D. Schladt, M. G. Samant and S. S. Parkin, *Science*, 2013, **339**, 1402-1405.
8. I. A. Verzhbitskiy, H. Kurebayashi, H. Cheng, J. Zhou, S. Khan, Y. P. Feng and G. Eda, *Nat. Electron.*, 2020, **3**, 460-465.
9. Z. Wang, T. Zhang, M. Ding, B. Dong, Y. Li, M. Chen, X. Li, J. Huang, H. Wang, X. Zhao, Y. Li, D. Li, C. Jia, L. Sun, H. Guo, Y. Ye, D. Sun, Y. Chen, T. Yang, J. Zhang, S. Ono, Z. Han and Z. Zhang, *Nat. Nanotechnol.*, 2018, **13**, 554-559.
10. D. Thureja, A. Imamoglu, T. Smolenski, I. Amelio, A. Popert, T. Chervy, X. Lu, S. Liu, K. Barmak, K. Watanabe, T. Taniguchi, D. J. Norris, M. Kroner and P. A. Murthy, *Nature*, 2022, **606**, 298-304.
11. L. A. Jauregui, A. Y. Joe, K. Pistunova, D. S. Wild, A. A. High, Y. Zhou, G. Scuri, K. De Greve, A. Sushko, C. H. Yu, T. Taniguchi, K. Watanabe, D. J. Needleman, M. D. Lukin, H. Park and P. Kim, *Science*, 2019, **366**, 870-875.
12. R. Y. Liu, Z. L. Wang, K. Fukuda and T. Someya, *Nat. Rev. Mater.*, 2022, **7**, 870-886.
13. Z. L. Wang and A. C. Wang, *Mater. Today*, 2019, **30**, 34-51.
14. D. J. Lacks and T. Shinbrot, *Nat. Rev. Chem.*, 2019, **3**, 465-476.
15. H. Wu, S. Wang, Z. Wang and Y. Zi, *Nat. Commun.*, 2021, **12**, 5470.
16. R. Lei, Y. Shi, Y. Ding, J. Nie, S. Li, F. Wang, H. Zhai, X. Chen and Z. L. Wang, *Energ. Environ. Sci.*, 2020, **13**, 2178-2190.
17. J. Cheng, W. Ding, Y. Zi, Y. Lu, L. Ji, F. Liu, C. Wu and Z. L. Wang, *Nat. Commun.*, 2018, **9**, 3733.
18. J. Nie, X. Chen and Z. L. Wang, *Adv. Funct. Mater.*, 2018, **29**, 1806351.
19. X. M. Li, P. Bista, A. Z. Stetten, H. Bonart, M. T. Schur, S. Hardt, F. Bodziony, H. Marschall, A. Saal, X. Deng, R. Berger, S. A. L. Weber and H. J. Butt, *Nat. Phys.*, 2022,

Published on 21 December 2023. Downloaded by the Georgia Tech Library on 1/2/2024 8:42:12 PM.

Energy & Environmental Science Accepted Manuscript

View Article Online
DOI: 10.1039/D3EE03496H

18, 713-719.
20. Q. Sun, D. Wang, Y. Li, J. Zhang, S. Ye, J. Cui, L. Chen, Z. Wang, H. J. Butt, D. Vollmer and X. Deng, *Nat. Mater.*, 2019, **18**, 936-941.
21. A. Li, Y. Zi, H. Guo, Z. L. Wang and F. M. Fernandez, *Nat. Nanotechnol.*, 2017, **12**, 481-487.
22. Z. Peng, J. Shi, X. Xiao, Y. Hong, X. Li, W. Zhang, Y. Cheng, Z. Wang, W. J. Li, J. Chen, M. K. H. Leung and Z. Yang, *Nat. Commun.*, 2022, **13**, 7835.
23. C. Zhang and Z. L. Wang, *Nano Today*, 2016, **11**, 521-536.
24. Y. Chen, Y. Zhang, Z. Wang, T. Zhan, Y. C. Wang, H. Zou, H. Ren, G. Zhang, C. Zou and Z. L. Wang, *Adv. Mater.*, 2018, **30**, 1803580.
25. D. Liu, X. Yin, H. Guo, L. Zhou, X. Li, C. Zhang, J. Wang and Z. L. Wang, *Sci Adv*, 2019, **5**, eaav6437.
26. C. Shan, W. Liu, Z. Wang, X. Pu, W. He, Q. Tang, S. Fu, G. Li, L. Long, H. Guo, J. Sun, A. Liu and C. Hu, *Energ. Environ. Sci.*, 2021, **14**, 5395-5405.
27. A. Chen, Q. X. Zeng, L. M. Tan, F. Xu, T. Y. Wang, X. F. Zhang, Y. L. Luo and X. Wang, *Energ. Environ. Sci.*, 2023, **16**, 3486-3496.
28. L. Zhou, D. Liu, Z. Zhao, S. Li, Y. Liu, L. Liu, Y. Gao, Z. L. Wang and J. Wang, *Adv. Energy. Mater.*, 2020, **10**, 2002920.
29. S. Fu, W. He, Q. Tang, Z. Wang, W. Liu, Q. Li, C. Shan, L. Long, C. Hu and H. Liu, *Adv. Mater.*, 2022, **34**, 2105882.
30. X. Fu, Y. Qin, Z. Zhang, G. Liu, J. Cao, B. Fan, Z. Wang, Z. Wang and C. Zhang, *Energy & Environmental Materials*, 2023, DOI: 10.1002/eem2.12566.
31. P. F. Chen, Y. J. Luo, R. W. Cheng, S. Shu, J. An, A. Berbille, T. Jiang and Z. L. Wang, *Adv. Energy. Mater.*, 2022, **12**, 2201813.
32. C. G. Zhang, Y. B. Liu, B. F. Zhang, O. Yang, W. Yuan, L. X. He, X. L. Wei, J. Wang and Z. L. Wang, *Acs Energy Letters*, 2021, **6**, 1490-1499.
33. S. Cui, L. Zhou, D. Liu, S. Li, L. Liu, S. Chen, Z. Zhao, W. Yuan, Z. L. Wang and J. Wang, *Matter*, 2022, **5**, 180-193.
34. J. Sun, L. Zhang, Z. Li, Q. Tang, J. Chen, Y. Huang, C. Hu, H. Guo, Y. Peng and Z. L. Wang, *Adv. Mater.*, 2021, **33**, e2102765.
35. P. Chen, J. An, S. Shu, R. Cheng, J. Nie, T. Jiang and Z. L. Wang, *Adv. Energy. Mater.*, 2021, **11**, 2003066.
36. W. He, W. Liu, J. Chen, Z. Wang, Y. Liu, X. Pu, H. Yang, Q. Tang, H. Yang, H. Guo and C. Hu, *Nat. Commun.*, 2020, **11**, 4277.
37. Q. J. Mu, W. C. He, C. C. Shan, S. K. Fu, S. H. Du, J. Wang, Z. Wang, K. X. Li and C. G. Hu, *Adv. Funct. Mater.*, 2023, DOI: 10.1002/adfm.202309421.
38. S. Niu, Y. S. Zhou, S. Wang, Y. Liu, L. Lin, Y. Bando and Z. L. Wang, *Nano Energy*, 2014, **8**, 150-156.
39. X. Zhang, M. Liu, Z. Zhang, H. Min, C. Wang, G. Hu, T. Yang, S. Luo, B. Yu, T. Huang, M. Zhu and H. Yu, *Small*, 2023, **19**, 2300890.
40. W. Paosangthong, M. Wagih, R. Torah and S. Beeby, *Nano Energy*, 2022, **92**, 106739.
41. T. Jiang, H. Pang, J. An, P. J. Lu, Y. W. Feng, X. Liang, W. Zhong and Z. L. Wang, *Adv. Energy. Mater.*, 2020, **10**, 2000064.
42. W. Shang, G. Q. Gu, F. Yang, L. Zhao, G. Cheng, Z.-l. Du and Z. L. Wang, *ACS Nano*,

Published on 21 December 2023. Downloaded by the Georgia Tech Library on 1/2/2024 8:42:12 PM.
Energy & Environmental Science Accepted Manuscript

2017, **11**, 8796-8803.

View Article Online
DOI: 10.1039/D3EE03496H

Published on 21 December 2023. Downloaded by the Georgia Tech Library on 1/2/2024 8:42:12 PM.

Energy & Environmental Science Accepted Manuscript

View Article Online
DOI: 10.1039/D3EE03496H

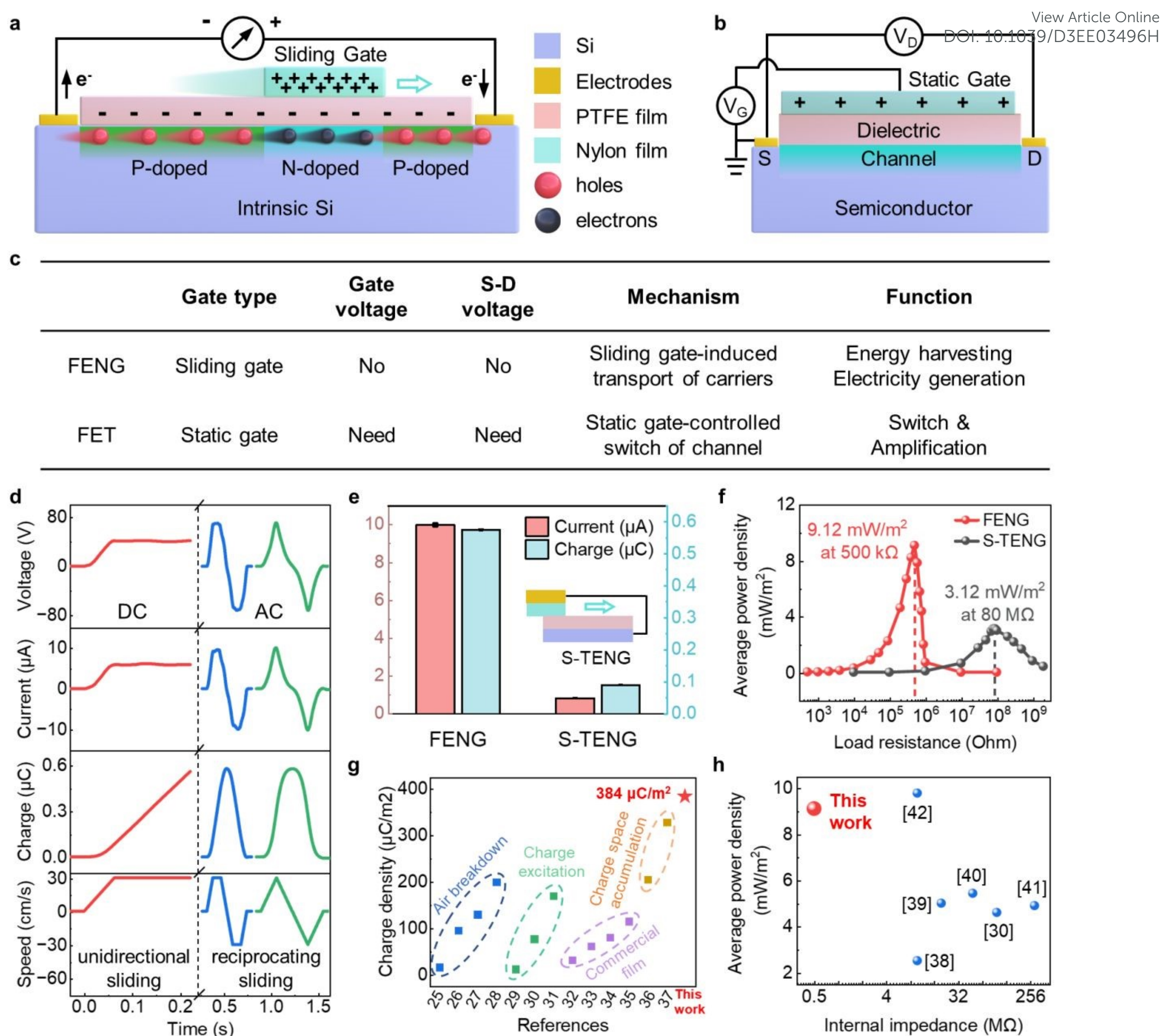

	Gate type	Gate voltage	S-D voltage	Mechanism	Function
FENG	Sliding gate	No	No	Sliding gate-induced transport of carriers	Energy harvesting Electricity generation
FET	Static gate	Need	Need	Static gate-controlled switch of channel	Switch & Amplification

Fig. 1. The structure and electric output of the FENG. (a) Structural schematic of the FENG device. **(b)** The structure of the FET device. **(c)** The comparison of our FENG device with the FET device. **(d)**The electric output characteristic of the FENG with different motion forms of slider. **(e)** The electric output comparison between FENG and control S-TENG device. **(f)** The comparison of average power density between FENG and control S-TENG device. **(g)** The comparison of transferred charge density of our FENG device with previous sliding or rotating TENGs in literature. **(h)** The comparison of average power density with previous sliding or rotating TENGs in literature. Note: The power and charge density were calculated by dividing the area of the entire stator or the covered area during the sliding process of the slider.

Published on 21 December 2023. Downloaded by the Georgia Tech Library on 1/2/2024 8:42:12 PM.

Energy & Environmental Science Accepted Manuscript

View Article Online
DOI: 10.1039/D3EE03496H

Published on 21 December 2023. Downloaded by the Georgia Tech Library on 1/2/2024 8:42:12 PM.

Energy & Environmental Science Accepted Manuscript

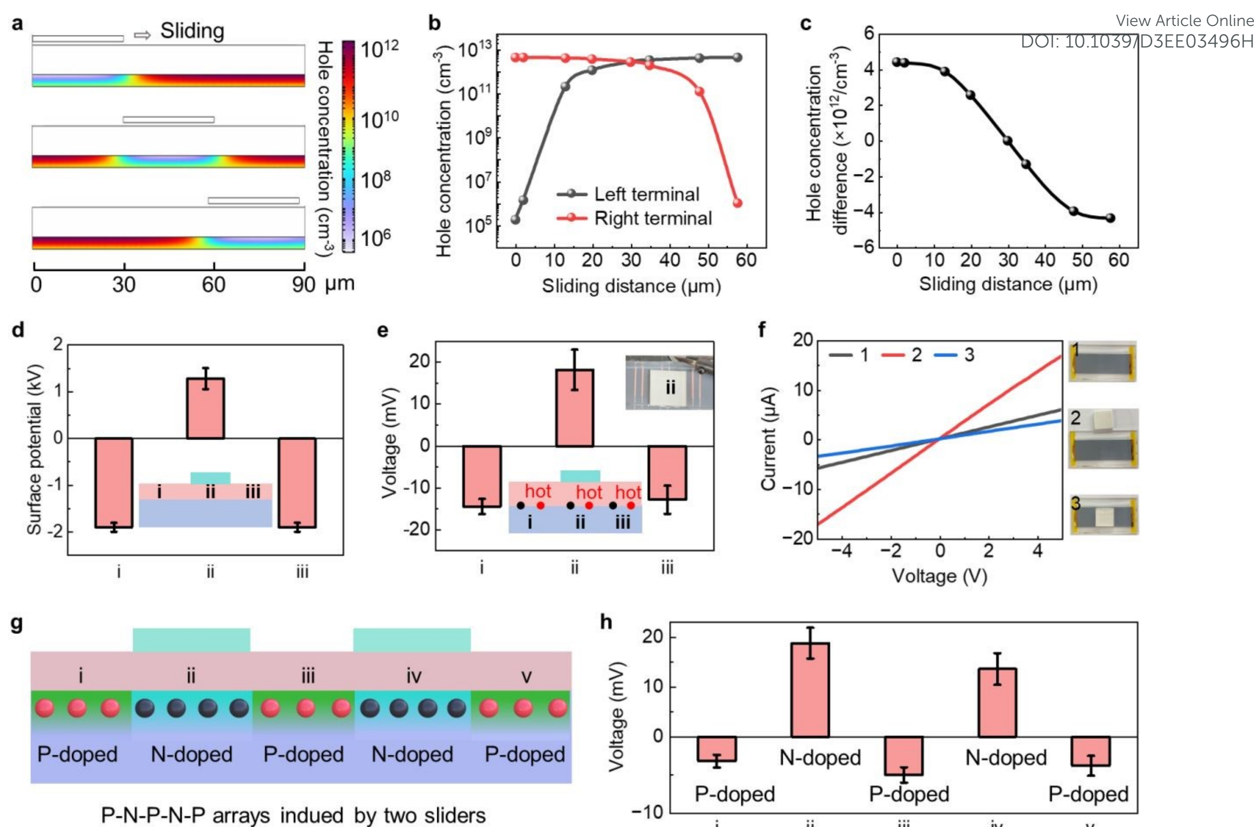

Fig. 2. The evidence of dynamical and regional doping of Si by electrostatic charges (the case of nylon film as slider). (a) The simulation of hole concentration distribution during the sliding of nylon film on the PTFE film. **(b)** The hole concentration at left and right electrodes with the sliding distance of nylon slider. **(c)** The hole concentration difference at left and right electrodes with the sliding distance of nylon slider. **(d)** The surface potential on the PTFE film at different regions. **(e)** The voltage due to the diffusion of hot carriers measured from three different regions of Si surface when nylon as slider. **(f)** The *I-V* curve of the Si channel when nylon as slider. **(g)** The schematic of P-N-P-N-P arrays induced by two sliders. **(h)** The voltage due to the diffusion of hot carriers of the five accordant regions.

View Article Online
DOI: 10.1039/D3EE03496H

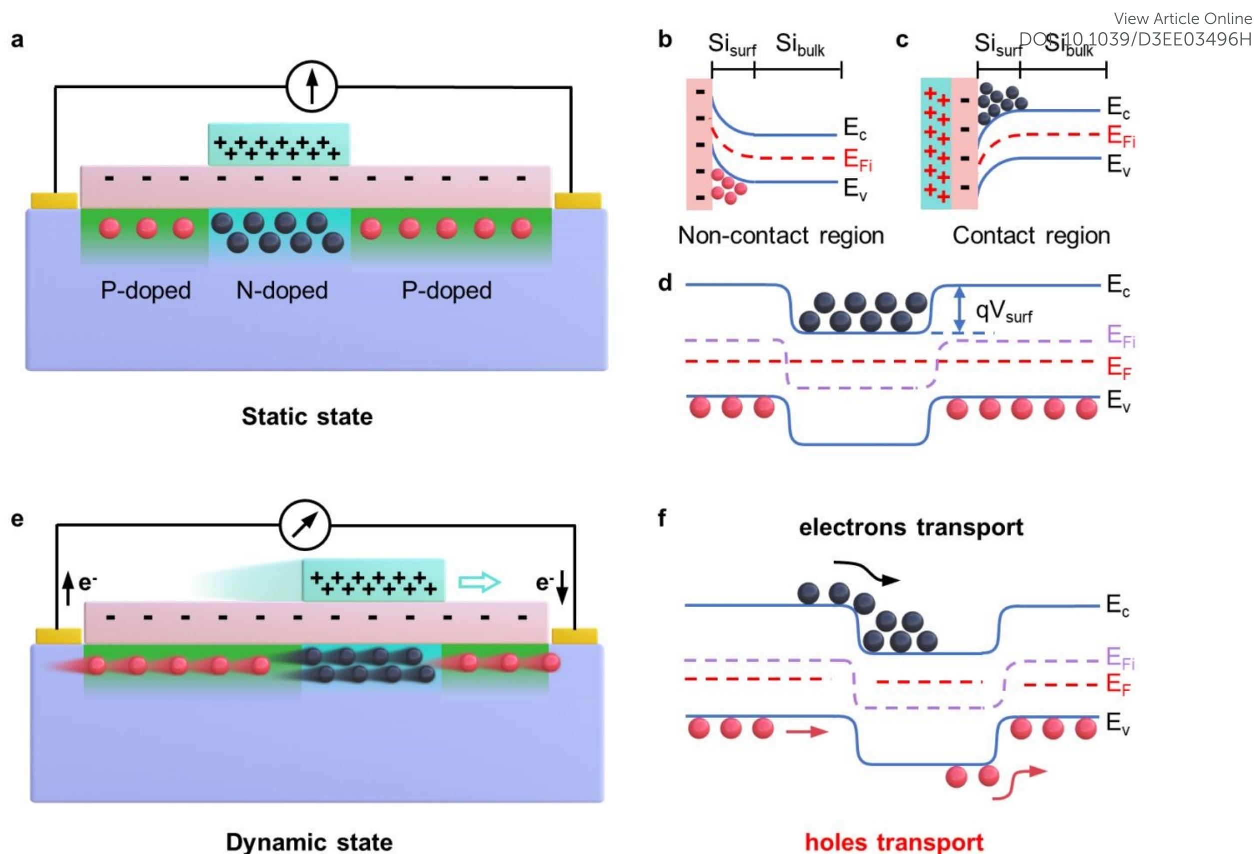

Fig. 3. The mechanism of the FENG device. (a) The schematic of the regional doping by electrostatic charges. **(b** and **c)** The energy band bending on the surface of Si at different regions, non-contact region (b) and contact region (c). **(d)** The energy band diagram of the whole surface Si "channel". **(e)** The schematic of charge carriers' transport in the Si "channel" induced by the dynamical electrostatic charges, leading to the electricity generation in external circuit. **(f)** The energy band diagram of the whole surface Si "channel" when sliding the nylon slider on the PTFE film.

Published on 21 December 2023. Downloaded by the Georgia Tech Library on 1/2/2024 8:42:12 PM.

Energy & Environmental Science Accepted Manuscript

View Article Online
DOI: 10.1039/D3EE03496H

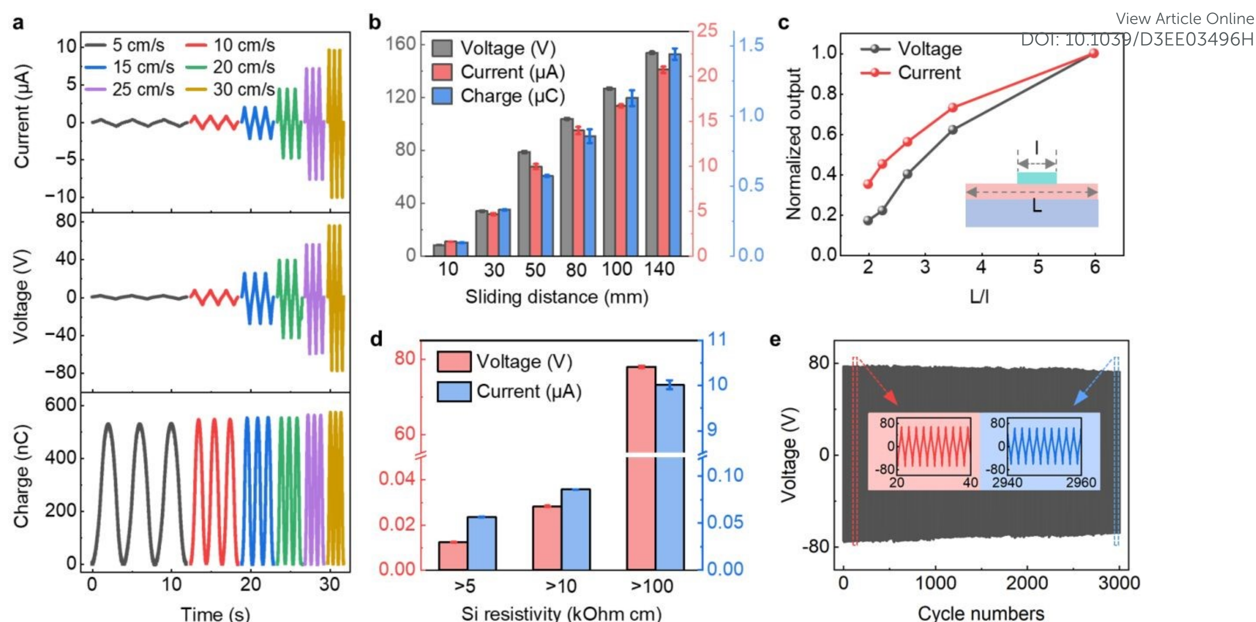

Fig. 4. The influencing parameters on the output of FENG device. (a) The influence of sliding speed of the nylon slider on the output of FENG device. **(b)** The influence of sliding distance of slider on the output of FENG device. **(c)** The influence of *L/l* ratio on the output of FENG. **(d)** The influence of the resistivity of Si on the output of FENG device. **(e)** The stability of the FENG device.

Published on 21 December 2023. Downloaded by the Georgia Tech Library on 1/2/2024 8:42:12 PM.

Energy & Environmental Science Accepted Manuscript

View Article Online
DOI: 10.1039/D3EE03496H

Published on 21 December 2023. Downloaded by the Georgia Tech Library on 1/2/2024 8:42:12 PM.

Energy & Environmental Science Accepted Manuscript

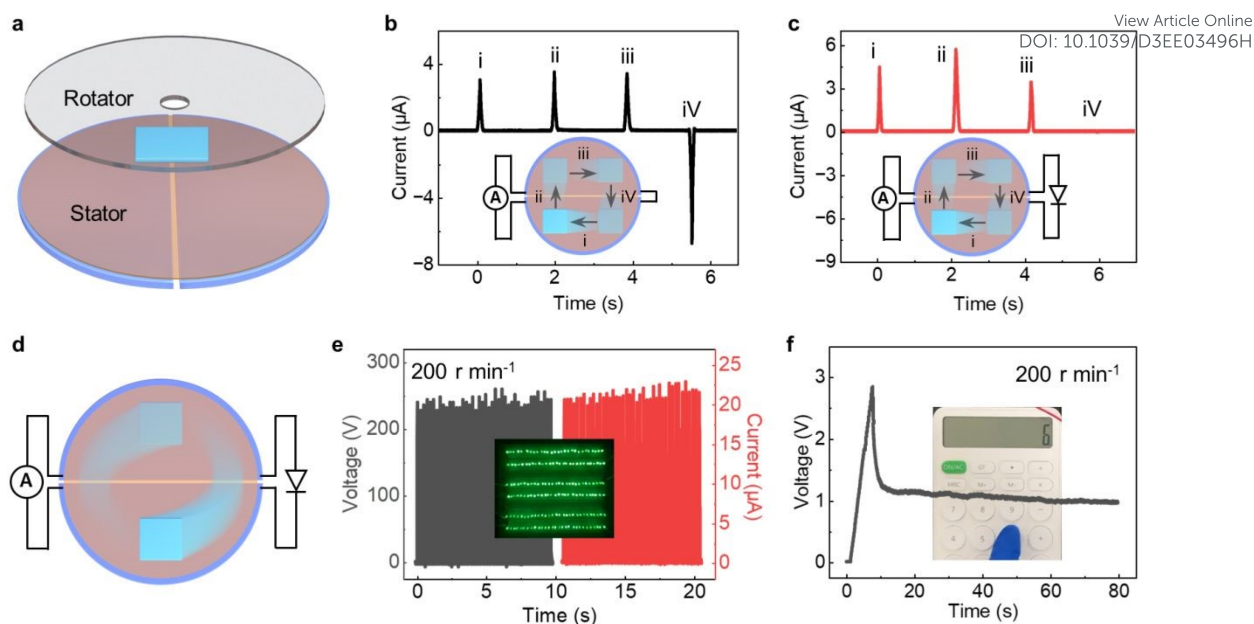

Fig. 5. The direct-current generation of a disc type FENG device. (a) The schematic of the disc type FET-TENG device. **(b** and **c)** The output characteristic of the disc type FENG device when the right sides of two semicircular Si are connected directly (b) and connected through a diode (c). The inset shows the sliding routes of the slider and the circuit connection. **(d)** The circuit connection of the disc type FENG device when the slider is in rotary sliding motion. **(e)** The output of disc type FENG at a rotating speed of 200 r min^{-1}. The inset shows 174 LEDs lighted up by the disc type FENG. **(f)** The voltage curve of a capacitor which is being charged by the FENG and, at the same time, powering a calculator continuously.